

On-surface synthesis of edge-extended zigzag graphene nanoribbons

Amogh Kinikar^{o a}, Xiushang Xu^{o b,c}, Marco Di Giovannantonio^{a,f}, Kristjan Eimre^{a,g}, Carlo A. Pignedoli^a, Klaus Müllen^{c,d}, Akimitsu Narita^{b,c}, Pascal Ruffieux^a, and Roman Fasel^{a,e}

^a Empa, Swiss Federal Laboratories for Materials Science and Technology, nanotech@surfaces Laboratory, 8600 Dübendorf, Switzerland

^b Okinawa Institute of Science and Technology Graduate University, Organic and Carbon Nanomaterials Unit, 1919-1 Tancha, Onnason, Kunigamigun, Okinawa 904-0495, Japan

^c Max Planck Institute for Polymer Research, 55128 Mainz, Germany.

^d Johannes Gutenberg University Mainz, Institute of Physical Chemistry, Duesbergweg 10-14, 55128 Mainz, Germany

^e University of Bern, Department of Chemistry, Biochemistry and Pharmaceutical Sciences, Freiestrasse 3, 3012 Bern, Switzerland

^o These authors contributed equally to this work.

Present address:

^fInstitute of Structure of Matter – CNR (ISM-CNR), via Fosso del Cavaliere 100, 00133 Roma

^gEPFL, École polytechnique fédérale de Lausanne, NCCR MARVEL, 1015 Lausanne, Switzerland

Contents

Supporting Information

S1: Nomenclature for edge-extended ZGNRs

S2: Synthesis and characterizations of monomer **6**

S3: Simulated dI/dV maps for a 9-unit segment of 3-ZGNR-E(Bisanthene, 7)

S4: Charging of the 3-ZGNR-E(Bisanthene, 7) on Au(111)

S5: NMR Spectra

Supporting Information

S1: Nomenclature for edge-extended ZGNRs

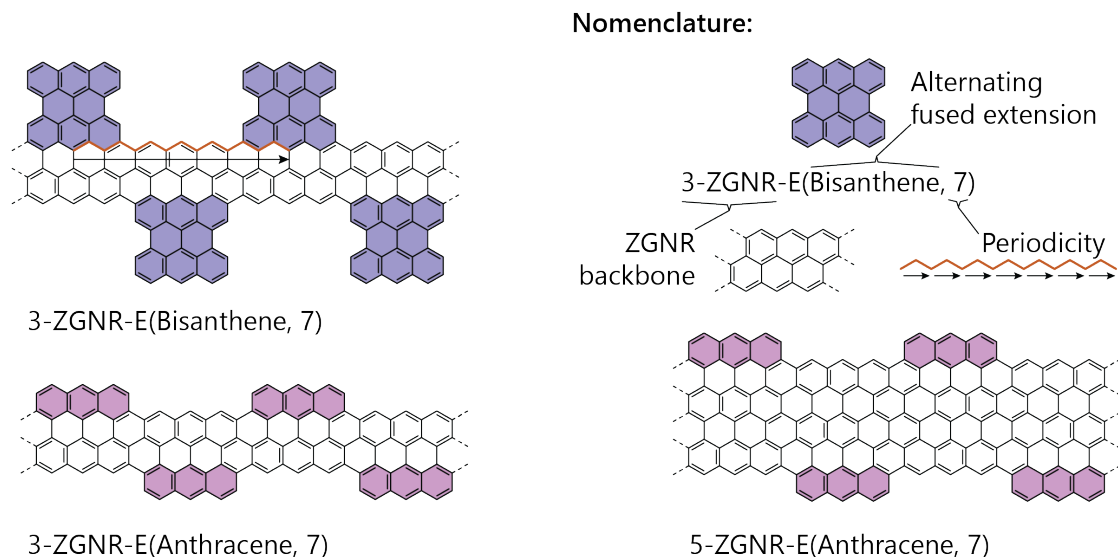


Figure S1: Nomenclature for edge-extended ZGNRs. The ZGNR backbone to which the extensions are fused is identified as the N zigzag rows wide ZGNR (N-ZGNR). The edge extensions that are fused to alternating sides of the N-ZGNR backbone are identified by their chemical name. The periodicity of the fused extensions along one edge is expressed in terms of the axial unit vector of the N-ZGNR. The nomenclature is illustrated with examples.

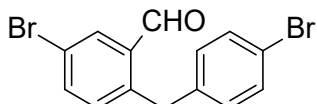
S2: Synthesis and characterizations of monomer 6

General Methods

All reactions working with air- or moisture-sensitive compounds were carried out under argon atmosphere using standard Schlenk line techniques. Unless otherwise noted, all starting materials and other chemicals were purchased from commercial sources and used without further purification. Thin-layer chromatography (TLC) was done on silica gel coated aluminum sheets with F254 indicator and column chromatography separation was performed with silica gel (particle size 0.063-0.200 mm). Nuclear Magnetic Resonance (NMR) spectra were recorded using Bruker DPX 300 MHz, Avance Neo 400/500 MHz NMR spectrometers. Chemical shifts (δ) were expressed in ppm relative to the residual solvents (CD_2Cl_2 , ^1H : 5.32 ppm, ^{13}C : 54.00 ppm; CDCl_3 , ^1H : 7.26 ppm, ^{13}C : 77.00). Coupling constants (J) were recorded in Hertz. Abbreviations: s = singlet, d = doublet, t = triplet, q = quartet, m = multiplet. High-resolution mass spectra (HRMS) were recorded on Electrospray ionization (ESI) Thermo Orbitrap Thermo Scientific LTQ-Orbitrap or on Bruker timsTOF atmospheric pressure chemical ionization (APCI) mass spectrometric (MS) detection.

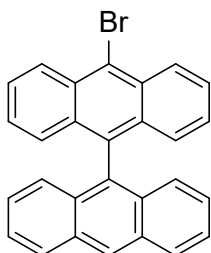
Synthesis Details

5-bromo-2-(4-bromobenzyl)benzaldehyde (**3**)



A 50-mL round flask was charged with 5-bromo-2-methylbenzaldehyde (1.20 g, 6.01 mmol), 1-bromo-4-iodobenzene (4.30 g, 15.0 mmol), silver trifluoroacetate (3.34 g, 15.0 mmol), glycine (360 mg, 4.80 mmol), palladium (II) acetate (136 mg, 0.601 mmol), and $\text{CH}_3\text{COOH}/\text{H}_2\text{O}$ (18 mL/2 mL). The reaction mixture was stirred at room temperature for 10 min and then at 100 °C for 36 h. The resulting mixture was cooled to room temperature, diluted with EtOAc (50 mL), and filtered through a silica gel plug. Then, organic phases were combined, washed with brine and saturated aqueous solution of NaHCO_3 , dried over MgSO_4 , and evaporated. The residue was purified by silica gel column chromatography (eluent: *n*-hexane: ethyl acetate = 20:1) to give the title compound (1.05 g, 52% yield) as light-yellow liquid. ^1H NMR (400 MHz, CDCl_3) δ 10.05 (s, 1H), 7.90 (d, J = 2.3 Hz, 1H), 7.58 (dd, J = 8.1, 2.2 Hz, 1H), 7.44 – 7.21 (m, 2H), 7.06 (d, J = 8.2 Hz, 1H), 6.92 (d, J = 8.4 Hz, 2H), 4.27 (s, 2H). ^{13}C NMR (126 MHz, CDCl_3) δ 190.82, 141.01, 138.60, 136.80, 135.27, 133.36, 131.78, 130.46, 121.19, 120.46, 37.05. HRMS (ESI, Positive): *m/z* Calcd. For ($\text{C}_{14}\text{H}_9\text{Br}_2$) $^+$: 334.9086, [M-OH] $^+$, found: 334.9059.

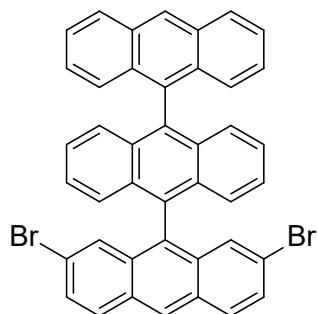
10-bromo-9,9'-bianthracene (**5**)



A round-bottom flask was charged with 9,9'-bianthracene (63 mg, 0.18 mmol), *N*-bromosuccinimide (NBS) (32 mg, 0.18 mmol), and THF (8.0 mL). After stirring at room temperature for overnight, the reaction was quenched with acetone (10 mL), and evaporated. The residue was purified by silica gel column chromatography (eluent: *n*-hexane: CH_2Cl_2 = 15:1) to give the title compound as yellow solid (31 mg, 40% yield). ^1H NMR (300 MHz, CDCl_3) δ 8.81 – 8.65 (m, 3H), 8.18 (d, J = 8.6 Hz, 2H), 7.62 – 7.57 (m, 2H), 7.47 (t, J = 7.5 Hz, 2H), 7.26 – 6.99 (m, 8H). ^{13}C NMR (75

MHz, CDCl₃) δ 133.96, 132.38, 132.33, 131.55, 131.49, 130.48, 128.60, 128.07, 127.58, 127.34, 127.19, 126.65, 126.12, 126.07, 125.40, 123.57. HRMS (ESI, Positive): *m/z* Calcd. For (C₂₈H₁₈Br)⁺: 433.0567, [M+H]⁺, found: 433.0586.

2,7-dibromo-9,9':10',9''-teranthracene (**6**)



To the solution of 10-bromo-9,9'-bianthracene (**5**) (300 mg, 0.694 mmol) in anhydrous diethyl ether (15 mL) at 0 °C under argon atmosphere, *n*-butyllithium (1.6 M in hexane, 0.5 mL, 0.8 mmol) was added dropwise. After stirring for 30 min at 0 °C, 5-bromo-2-(4-bromobenzyl)benzaldehyde (244 mg, 0.694 mmol) in dry diethyl ether (10 mL) was added. The resulting mixture was stirred at room temperature overnight, and then quenched with methanol (1.0 mL). After stirring for 10 min, the mixture was extracted with CH₂Cl₂ (20 mL) for three times. The organic phases were combined, washed with brine, dried over MgSO₄, and evaporated. The resulting crude product was dissolved in anhydrous CH₂Cl₂ (10 mL) and BF₃·OEt₂ (0.2 mL) was added at 0 °C. The reaction mixture was allowed to warm to room temperature and stirred for 2 h, and then quenched with the saturated aqueous solution of NaHCO₃ (10 mL). The organic phase was separated, dried over MgSO₄, and evaporated. The cyclization product was dissolved in anhydrous CH₂Cl₂ (10 mL) and 2,3-dichloro-5,6-dicyano-1,4-benzoquinone (DDQ) (157 mg, 0.694 mmol) was subsequently added to the solution. The resulting mixture was stirred at room temperature for 2 h, and then was poured into water (20 mL), followed by extraction with CH₂Cl₂ (20 mL) for three times. Then, organic phases were combined, washed with brine, dried over MgSO₄, and evaporated. The residue was purified by silica gel column chromatography (eluent: *n*-hexane: CH₂Cl₂ = 10:1) to give the title compound (310 mg, 65% yield) as white solid. ¹H NMR (400 MHz, CD₂Cl₂) δ 8.84 (s, 1H), 8.80 (s, 1H), 8.29 (d, *J* = 8.6 Hz, 2H), 8.16 (d, *J* = 9.0 Hz, 2H), 7.65 (d, *J* = 9.0 Hz, 2H), 7.59 – 7.57 (m, 2H), 7.38 – 7.34 (m, 4H), 7.35 (d, *J* = 3.4 Hz, 2H), 7.29 – 7.26 (m, 6H). ¹³C NMR (126 MHz, CD₂Cl₂) δ 134.78, 133.07, 132.87, 132.06, 131.93, 131.71, 131.68, 131.55, 131.47, 130.68, 130.09, 129.50, 128.74, 128.34, 128.19, 127.57, 127.26, 126.71, 126.63, 126.22, 126.15, 125.89, 125.49, 121.41. HRMS (APCI, Positive): *m/z* Calcd. For (C₄₂H₂₅Br₂)⁺: 687.0323, [M+H]⁺, found: 687.0318.

S3: Simulated dI/dV maps for a 9-unit segment of 3-ZGNR-E(Bisanthene, 7)

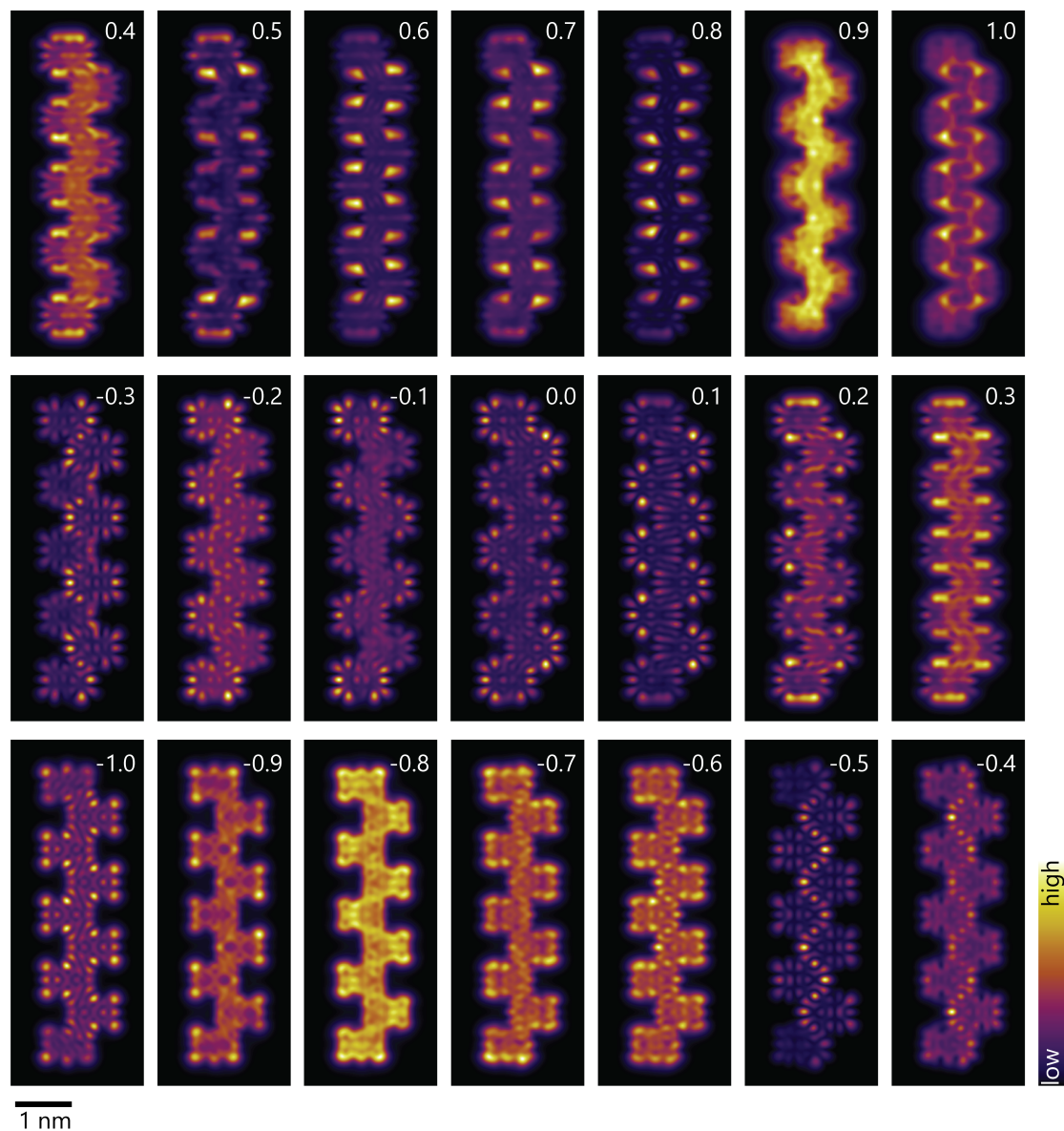


Figure S2: Extended dI/dV simulations of the system in Fig. 4 of the main text are provided for reference. The bias at which the simulation was performed is indicated in eV inside each dI/dV map. dI/dV maps are simulated at a constant-height of 4 Å above the GNR.

S4: Charging of the 3-ZGNR-E(Bisanthene, 7) on Au(111)

Projected density of states¶

Here, we provide a didactic discussion on the projected density of states (PDOS).

Let the molecule be defined by: $H_M = \begin{bmatrix} M_1 & \cdots & 0 \\ \vdots & \ddots & \vdots \\ 0 & \cdots & M_p \end{bmatrix}$ with $|M_i\rangle$ as the eigenvectors with M_i eigenvalues. Each gas-phase molecular orbital would be one eigenvector.

We can define the Hamiltonian and eigenvectors for the substrate as: $H_S = \begin{bmatrix} S_1 & \cdots & 0 \\ \vdots & \ddots & \vdots \\ 0 & \cdots & S_q \end{bmatrix}$ and $|S_i\rangle$.

The combined Hamiltonian of the molecule and the slab in a correspondingly expanded Hilbert basis would be: $H_C = \begin{bmatrix} H_M & T \\ T^\dagger & H_S \end{bmatrix}$ with $|C_i\rangle$ as the eigenvectors, where T is a $p \times q$ matrix that introduces the coupling between the substrate and the molecule, with T^\dagger as its transpose conjugate.

When there is no coupling between the molecule and the slab: $T = 0_{p \times q}$. In this scenario, H_C is a diagonal matrix, and its eigenvectors are simply those of the molecule and the substrate (expressed in the expanded Hilbert space):

$$|C^0_i\rangle = \begin{cases} |M_i\rangle, & i \leq p \\ |S_{i-p}\rangle, & p < i \leq p+q \end{cases}$$

Moreover, these eigenvectors are also orthonormal to each other. The dot product of the gas-phase molecular orbitals (expressed in the expanded Hilbert space) onto the eigenvectors of the molecule and the substrate is:

$$\sum_i^{p+q} |C^0_i\rangle \langle C^0_i | M_j \rangle$$

However, as $|C^0_i\rangle = |M_i\rangle$ for $i \leq p$:

$$\therefore \langle C^0_i | M_j \rangle = \delta_{ij}$$

The above result is trivial. We have shown that molecular orbitals map to themselves when they do not hybridize with the surface. However, if the molecule and the slab can hybridize, T is not a null matrix and H_C is no longer diagonal. Therefore, the eigenvectors of the coupled system, $|C^{hy}_i\rangle$ are in general:

$$|C^{hy}_i\rangle = \sum_k n_k^i |C^0_k\rangle$$

with $\sum_k |n_k^i|^2 = 1$ for normalization. Therefore, the dot product of the gas-phase molecular orbitals with all states of the hybridized molecule and slab system is:

$$\begin{aligned} \sum_i^{p+q} |C^{hy}_i\rangle \langle C^{hy}_i | M_j \rangle &= \sum_i^{p+q} |C^{hy}_i\rangle \sum_k n_k^i \langle C^0_k | M_j \rangle \\ \Rightarrow \langle C^{hy}_i | M_j \rangle &= \sum_k n_k^i \langle C^0_k | M_j \rangle \\ \therefore \langle C^{hy}_i | M_j \rangle &= n_j^i \end{aligned}$$

Thus upon hybridization, the j^{th} gas-phase molecular orbital can have non-zero projections on all states of the adsorbed molecule-on-slab system.

As the $|C^{hy}_i\rangle$ form an orthonormal basis set: $\sum_i |n_j^i|^2 = 1$.

Therefore $|n_j^i|^2$ is a probability mass function. Since the slab is large, we can treat the discrete energy eigenvalues labeled with the variable i as a continuous function of energy. Thus, $|n_j^i|^2$ can then be expressed as a probability density function: $\int_{-\infty}^{\infty} n_j(E) \cdot dE = 1$.

This probability density function $n_j(E)$ is the projected density of states (PDOS) of the j^{th} molecular orbital projected onto the hybridized system. PDOS is a useful parameter to reflect the hybridization of orbitals. For a non-hybridized system:

$$n_j(E) = \delta(E - M_j)$$

Any hybridization would broaden the delta function.

Moreover, consider if instead of hybridization between the substrate and the molecules, there was simply a rigid shift in the energy of the molecular orbitals when the molecule is adsorbed on the system:

$$H_C = \begin{bmatrix} H_M + u \cdot \mathbb{I} & 0 \\ 0 & H_S \end{bmatrix}$$

In such a scenario, $\langle C^0_i | M_j \rangle = \delta_{ij}$ would still be valid. However:

$$\langle C^0_i | H_C | C^0_i \rangle = \begin{cases} M_i + u, & i \leq p \\ S_i, & p < i \leq p + q \end{cases}$$

The PDOS in this situation would be:

$$n_j(E) = \delta(E - (M_j + u))$$

Thus, the peak of the PDOS can also reflect the shift in the energy of the orbitals once they have adsorbed on the surface.

The PDOS for the gas phase orbitals of the 9-unit 3-ZGNR-E(BA , 7)a segment and the adsorbed same segment adsorbed on an Au(111)-slab are shown in Fig. S5. Most orbitals reveal a significantly broadened PDOS revealing a clear hybridization with the surface. Hole doping induced by interaction with the surface is evidenced by systematic shifts of the prominent peak of each PDOS to higher energy than the corresponding gas-phase orbital. Consequently, the HOMO, HOMO-1, and HOMO-2 are substantially depopulated, thus rendering the GNR closed shell.

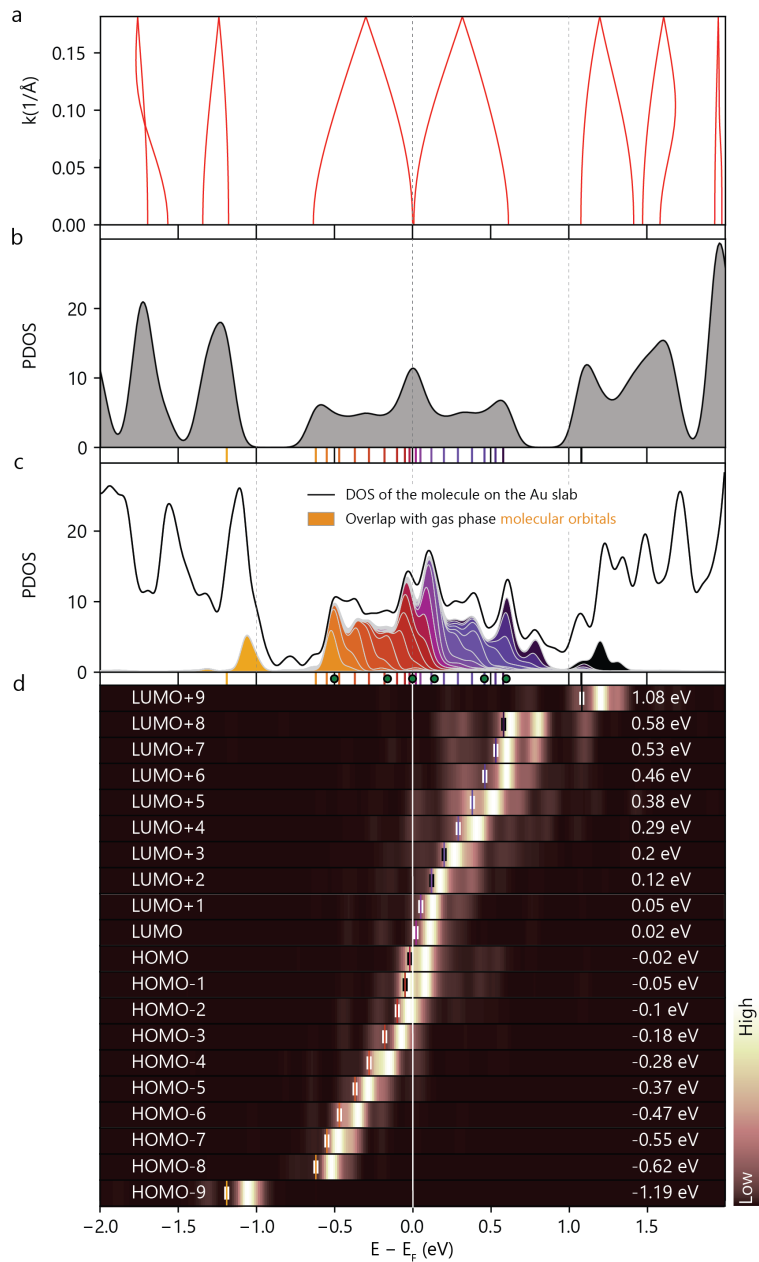


Figure S3: Hybridization of the GNR orbitals with the Au slab. **a**, Gas phase DFT band structure of the 3-ZGNR-E(Bisanthene, 7). **b**, The corresponding gas-phase density of states (DOS). **c**, Total DOS (black line) of a 3-ZGNR-E(BA, 7) segment consisting of 9 precursor units adsorbed on Au(111). PDOS of 10 occupied (HOMO to HOMO-9) and 10 unoccupied (LUMO to LUMO+9) orbitals are shown in colored overlaid peaks. The energies of all the calculated orbitals are indicated by colored lines on the x-axis of panels **b** and **c**. For reference, the energies of the simulated dI/dV maps shown in Fig. 4 of the main text are indicated by green dots below the x-axis. **d**, Color maps representing the PDOS as a function of energy for the different orbitals. Colored short vertical lines indicate the gas-phase energy of the corresponding orbital; these are also written on the right-hand-side.

S5: NMR Spectra

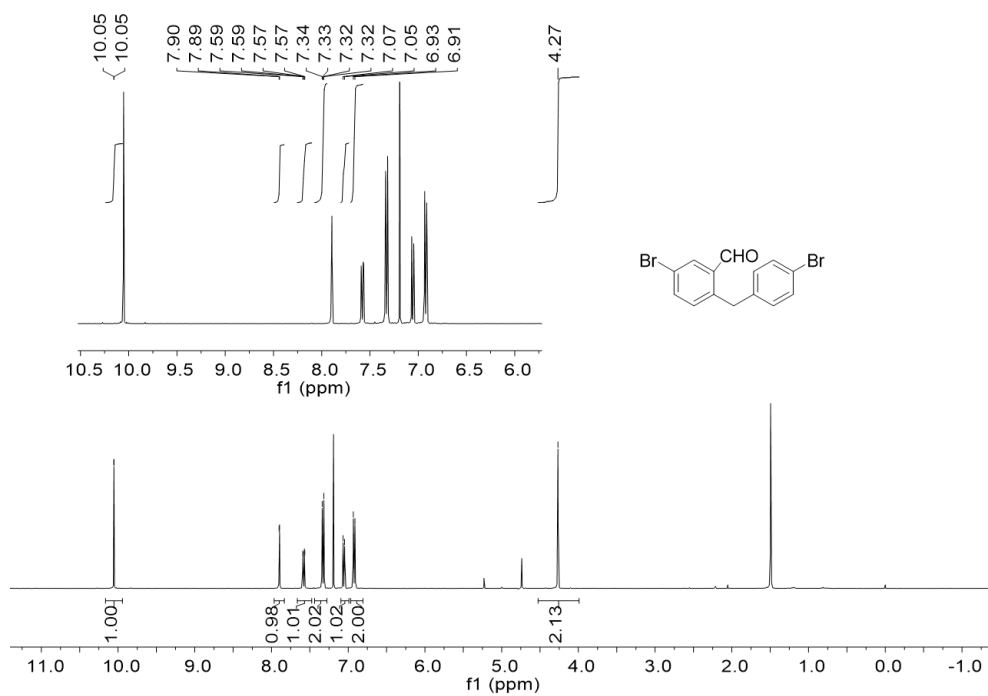


Figure S4. ¹H NMR spectrum of compound **3** in CDCl₃ (400 MHz, 298 K).

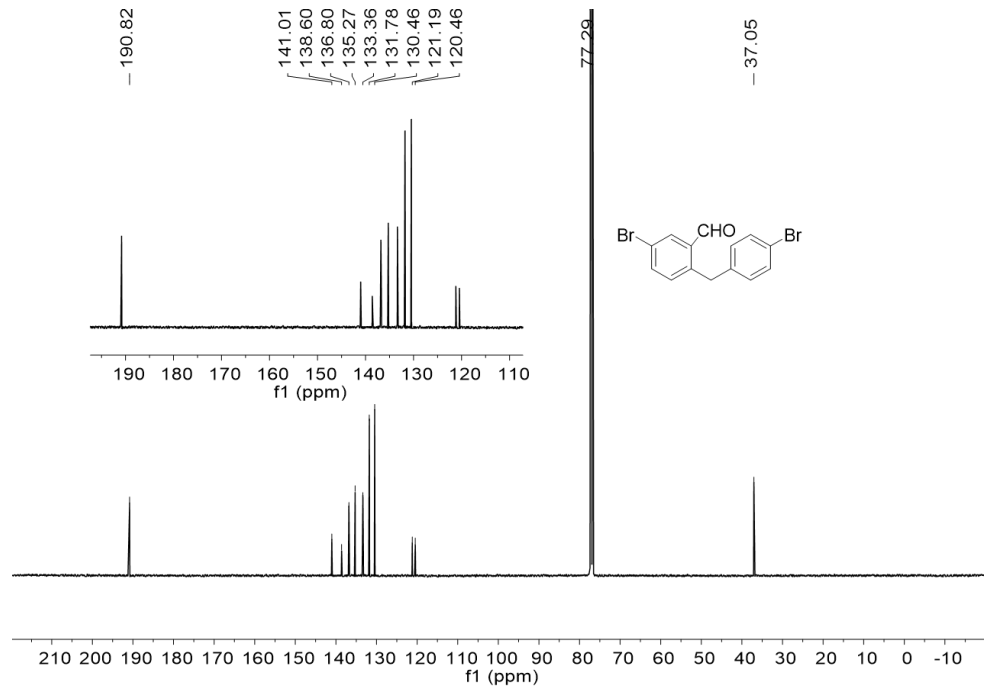


Figure S5. ¹³C NMR spectrum of compound **3** in CDCl₃ (126 MHz, 298 K).

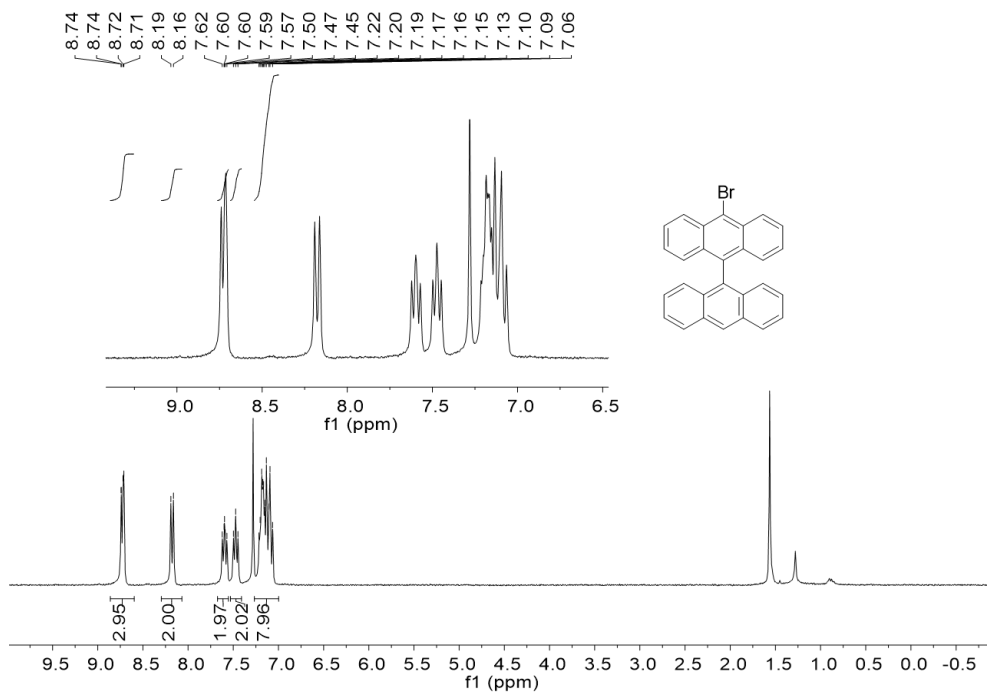


Figure S6. ^1H NMR spectrum of compound **5** in CDCl_3 (300 MHz, 298 K).

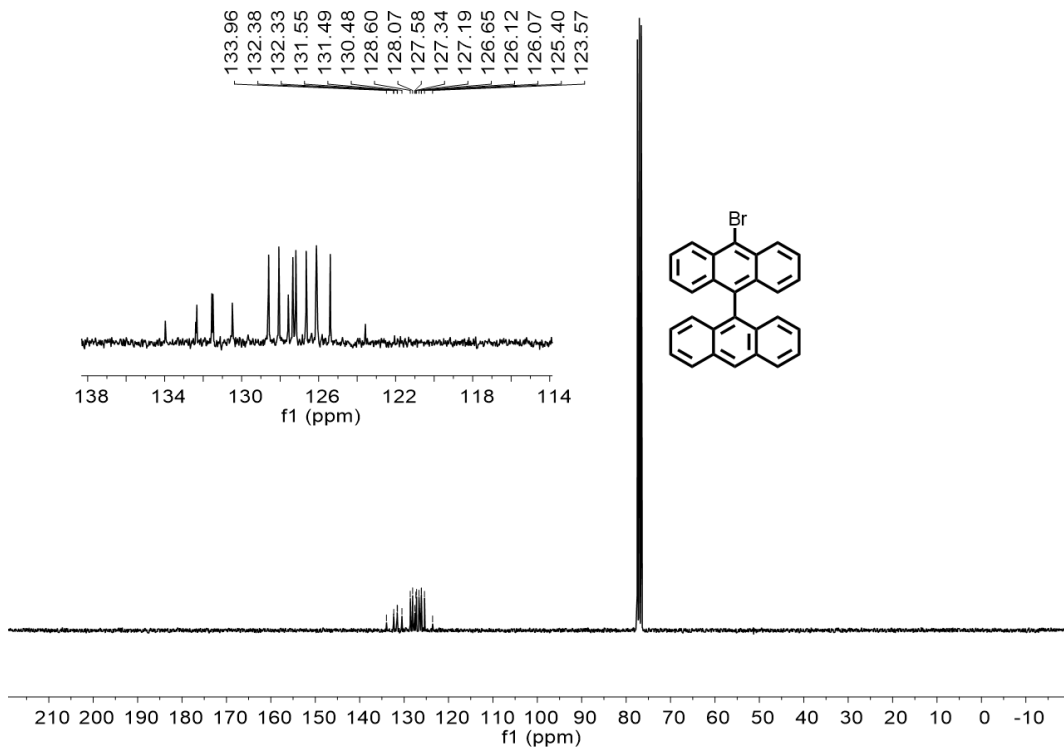


Figure S7. ^{13}C NMR spectrum of compound **15** in CDCl_3 (75 MHz, 298 K).

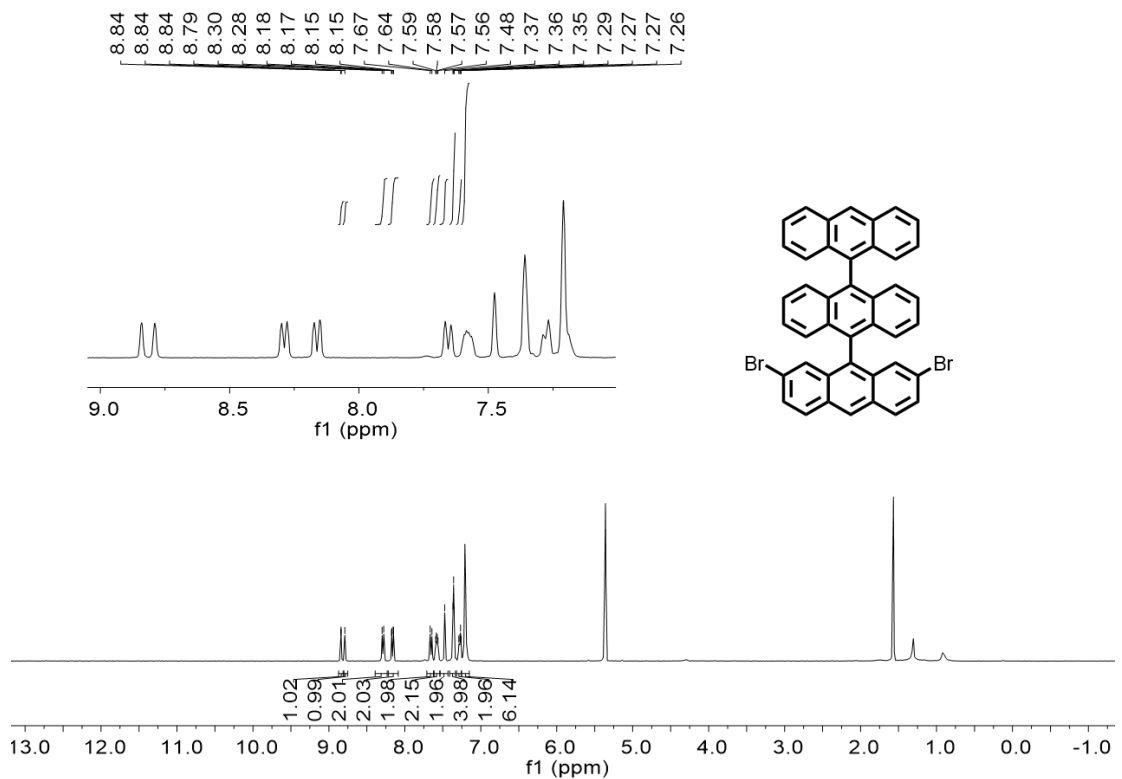


Figure S8. ^1H NMR spectrum of compound **10** in CD_2Cl_2 (400 MHz, 298 K).

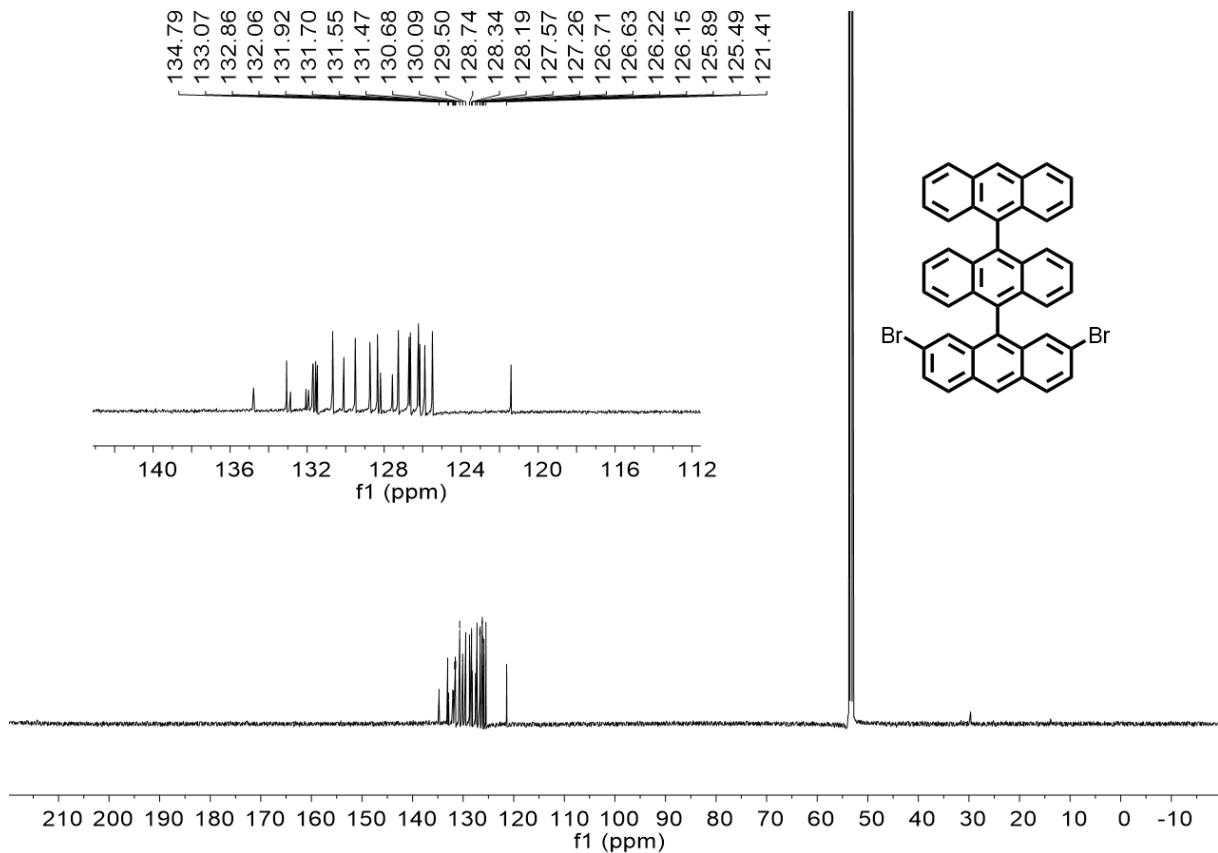


Figure S9. ^{13}C NMR spectrum of compound **10** in CD_2Cl_2 (126 MHz, 298 K).